Astronomy Reports, vol. 51, No.11, 2007, pp.871-881 February 2, 2008
Translated from Astronomicheskii Zhurnal, vol.84, No.11, 2007, pp. 963-974

arXiv:0711.2313v1 [astro-ph] 14 Nov 2007

The gas emission spectrum in a star-forming region in the BCD galaxy VII Zw 403 (UGC 6456)

V.P. Arkhipova[1], T.A. Lozinskaya[1], A.V. Moiseev[2], and O.V. Egorov[1]

[1] Sternberg Astronomical Institute, Universitetskii pr. 13, Moscow, 119992 Russia
[2] Special Astrophysical Observatory, RAS, Nizhnii Arkhyz, Karachai-Cherkessian Republic, 357147 Russia

Abstract. Observations with the 6-m telescope of the Special Astrophysical Observatory obtained with the MPFS integral-field spectrograph and a longslit spectrograph with the SCORPIO focal reducer are used to analyze the emission spectrum of the ionized gas in a star-forming region in the BCD galaxy VII Zw 403. We present images of the galactic central region in the Hα, Hβ, [SII], and [OIII] emission lines, together with maps of the relative [OIII]/Hβ and [SII]/Hα intensities. We have determined the parameters of the gas in bright ionized supershells, and estimated the relative abundances of oxygen, nitrogen, and sulfur; a low relative N/O abundance was detected.

1. Introduction

Indications of active star formation in blue compact dwarf (BCD) and Irr galaxies include giant complexes containing most of the young stellar population, bright HII regions, and multiple shells and supershells of various sizes. Such complexes clearly reveal interaction of OB associations with the ambient gas, providing unique possibility for observational verification of the classic theory of interaction of collective winds and supernovae with the interstellar medium, which is so far in a fairly poor agreement with observations.

This paper continues studies of the interstellar medium in a complex associated with a recent burst of star formation in the BCD galaxy VII Zw 403 (UGC 6456) initiated by Lozinskaya et al. [1].

VII Zw 403 is one of the closest BCD galaxies (at the distance $d = 4.5$ kpc), is isolated and slowly rotating and has undergone several star-formation episodes of various intensities [2,3]. The most recent burst of star formation happened 4–10 Myr ago and encompassed a central region of the galaxy, about one kpc in size, in the direction of a giant neutral hydrogen cloud with a very high column density [4].

Several sites associated with this latest star-formation episode are observed; the youngest massive stars form compact OB associations Nos. 1-6 (for uniformity, like in [1], we use the notation for associations and HII regions of Lynds et al. [2]). More evolved stars, including high-luminosity red supergiants, are distributed in an extended, elliptical area and show no concentration toward the compact associations. The ionized gas is concentrated in the same central region of the galaxy, and exhibits signs of several sites of recent star formation, in the form of bright HII regions associated with compact associations and faint diffuse emission surrounding them [2, 5, 6]. Observations with the HST have revealed shell-like structures 80-100 pc in size for a number of bright HII regions. Lynds et al. [2] used slit spectrograms obtained on the 4-m telescope of the Kitt Peak National Observatory to derive the shells expansion rate, $50-70\,\mathrm{km\,s^{-1}}$, although these results were not confirmed by Lozinskaya et al. [1] (see below). Silich et al. [7] found traces of a giant ($D \simeq 500$ pc), faint ring in Hα emission produced by diffuse gas. Reports of the presence of an extended region of diffuse X-ray emission inside this giant ring remain, for the moment, unconfirmed [8-12].

In our paper [1], we presented a detailed study of the large-scale structure and kinematics of the ionized gas using observations obtained on the 6-m telescope of the Special Astrophysical Observatory (SAO) Russian Academy of Sciences with the SCORPIO multi-mode focal reducer in three modes: direct imaging (in the Hα, [OIII], and [SII] lines), longslit spectroscopy, and spectroscopy with a scanning scanning Fabry–Perot interferometer. In addition to the known bright HII regions and traces of the faint giant ring, we detected many new diffuse and ring structures, detected fine structure in the giant ring, and mapped the radial-velocity distribution at the maximum and half-maximum levels of the Hα line for the entire central region of the galaxy. To search for signs of expansion, we plotted so-called 'velocity ellipses' and distributions of the half-width of the Hα line for all the HII regions; however, we found no variations of the radial

Send offprint requests to: T.A. Lozinsksaya, e-mail: lozinsk@sai.msu.ru

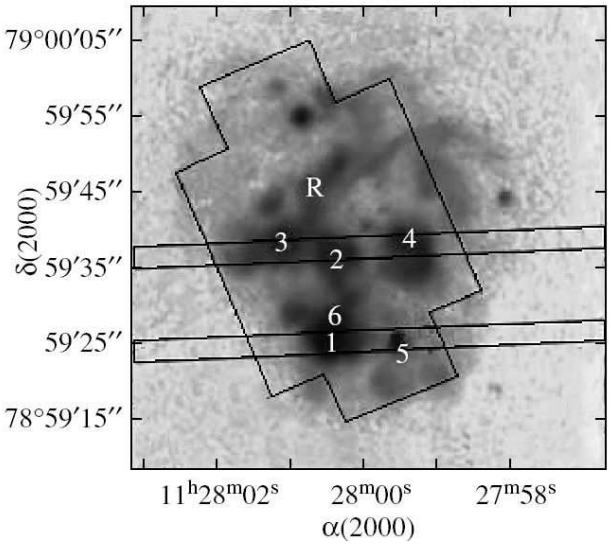

Fig. 1. Direct Hα image of the region of current star formation from [1]. The part of the galaxy covered by the MPFS observations and the positions of the spectrograph slit are shown. The numbers mark the bright HII regions noted in the Introduction (according to the designations of Lynds et al. [2]), the letter R marks the brightest part of the giant ring.

velocity at the line maximum and/or halfwidths providing evidence for expansion of the shells with a velocity of $50-70\,\mathrm{km\,s^{-1}}$, as reported in [2]. Our longslit spectrograph observations in the red (Hα, [NII], [SII]) and green (Hβ, [OIII]) ranges likewise did not reveal any indications of the shells expansion with such velocities. On the contrary, our Fabry-Perot interferometer and longslit spectrograph data displayed an obvious line that broadened (from FWHM $\simeq 60-70\,\mathrm{km\,s^{-1}}$ to FWHM $\simeq 80-120\,\mathrm{km\,s^{-1}}$) in the region of the faint, diffuse emission outside the bright HII regions.

The kinematic age of the bright shells corresponding to our estimates of their expansion velocity ($20\,\mathrm{km\,s^{-1}}$ or lower) is at least 2-4 Myr, in good agreement with the ages of the corresponding compact OB associations estimated in [2]. The extended filamentary and diffuse regions of ionized gas detected essentially throughout the central part of the galaxy and the giant HII ring could be related to the older star population from the most recent burst of star formation (with an age of 10 Myr, according to [2]). We demonstrated in [1] based on our direct images that the large-scale structure of the star-forming region was generally the same in the [OIII], [SII], and Hα + [NII] lines. In two extended, very faint, diffuse regions, we found enhanced relative [OIII]/Hα and [SII]/Hα line intensities. However, due to the low brightness of these diffuse regions, these preliminary conclusions needed to be checked using observations with an integra-field (3D, panoramic) multi-pupil fiber spectrograph. In the brightest shell (No. 1) around the richest and youngest association (No. 1), we detected in [1] the presence of weak high-velocity wings: in the [OIII] line, out to velocities from -200 to $-300\,\mathrm{km\,s^{-1}}$ from the line center for intensities of 5% of the line maximum, and in the Hα line, out to $-350\,\mathrm{km\,s^{-1}}$ and $550-600\,\mathrm{km\,s^{-1}}$ for intensities of about 2% of the line maximum. This was the first detection of velocities this high in this galaxy, and provides clear evidence for acceleration of gas at shock fronts. Panoramic spectrograph observations are of special interest for shell No. 1.

Table 1. Log of MPFS spectroscopy.

Field	Date	$T_{\rm exp}$, s	Seeing, $''$
1	2004 May 23/24	1800	2.0
2	2004 May 23/24	1800	2.0
3	2004 May 24/25	1800	1.7
4	2004 May 24/25	1800	1.7
5	2004 May 24/25	1200	1.7
6	2004 May 24/25	1200	1.7
7	2004 May 24/25	600	1.7

In the present study, we analyze the emission spectrum of the gas in the star-formation region using observations of the galaxy obtained with the integral-field multi-pupil fiber spectrograph (MPFS) and longslit spectrograph of the SAO 6-m telescope. We present our observations and reduction techniques in the next section, followed by the main results of the observations and a discussion and conclusions.

2. Observations and data reductions

2.1. Observations with the MPFS

Our observations with the integral-field spectrograph MPFS at the primary focus of the SAO 6-m telescope were made on May 23/24 and 24/25, 2004. A description of the spectrograph is given by Afanasiev et al. [13] or at web-address `http://www.sao.ru/hq/lsfvo/devices.html`. The detector was a 2048×2048-pixel EEV 42-20 CCD chip. The spectrograph enables the recording of spectra from 256 spatial elements (designed as square lenses), forming an array of 16×16 elements in the sky plane. The scale was $1''$ per lens. Simultaneously, we recorded the night-sky spectrum of a field at a $4'$ distance from the center of MPFS field of view. The spectra had a resolution of about 8 Å and covered the wavelegth range 4250−7200 Å. In total, we observed seven fields in the galactic central region, displaced with respect of each other. Table 1 presents the total exposure time, $T_{\rm exp}$, and the mean seeing for each of the fields.

We reduced our spectral observations using IDL-based software developed in the SAOs Laboratory of Spectroscopy and Photometry of Extragalactic Objects by V. Afanasiev and A. Moiseev. The primary reduction included bias subtraction, flat-fielding, removal of cosmic-ray hits, extraction of individual spectra in the CCD images, and wavelength calibration using the spectrum of a He-Ne-Ar calibration lamp. The night-sky spectrum

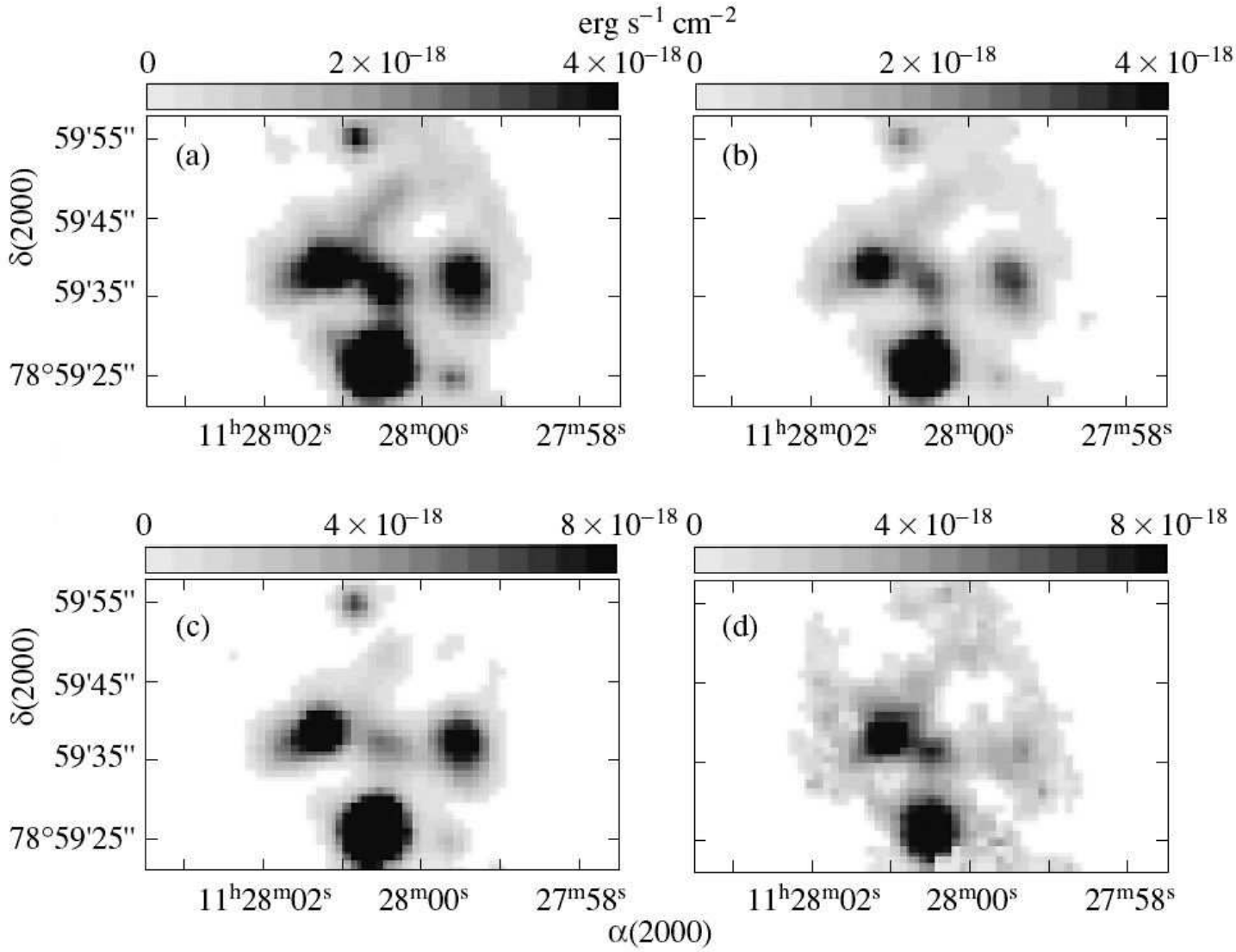

Fig. 2. Images of the central part of the galaxy in the (a) Hα, (b) Hβ, (c) [SII]λ6717 + 6731Å (c), and (d) [OIII]λ5007Å lines from MPFS observations.

was subtracted from the linearized spectra. The observed fluxes were then expressed in an absolute energy scale using spectra of the spectrophotometric standard Grw+70 5824, which was observed immediately after VII Zw 403 at a similar zenith distance. We used the mean atmospheric-extinction spectral curve for the SAO given in [14] to carry out air-mass corrections.

The data reduction yields a data cube, with each 16×16 pixel of the image represented by a spectrum of 2048 elements. After the preliminary reduction, the data cubes for all seven fields were put together and summed, so that the resulting mosaic had a size of $49'' \times 31''$; the corresponding region of the galaxy is shown in Fig. 1.

2.2. Longslit spectra

In this paper, we use the spectra analyzed in [1] to study the emission characteristics in individual lines. A log of our observations and a description of the instrument and data-reduction techniques are given in [1]. Here, we only briefly note that the observations were acquired at the prime focus of the SAO 6-m telescope with the SCORPIO multi-mode instrument [15]. We obtained two spectra (slit positions are shown in Fig. 1: section 1 passed through HII regions Nos. 2, 3, and 4 and section 2 through regions Nos. 1 and 5. In both cases, the position angle of the spectrograph slit was 88°. The spectra were recorded in two spectral ranges, corresponding to $\lambda\lambda$4800−5600 Å which includes the bright Hβ and [OIII] lines, and $\lambda\lambda$6270−7300 Å, which contains the Hα , [NII], and [SII] lines. The spectral resolution was 2.2−2.5 Å.

3. Results

Figure 1 presents the direct Hα image of the star-formation region in the galaxy obtained in [1]; the numbers correspond to the bright HII regions mentioned in the

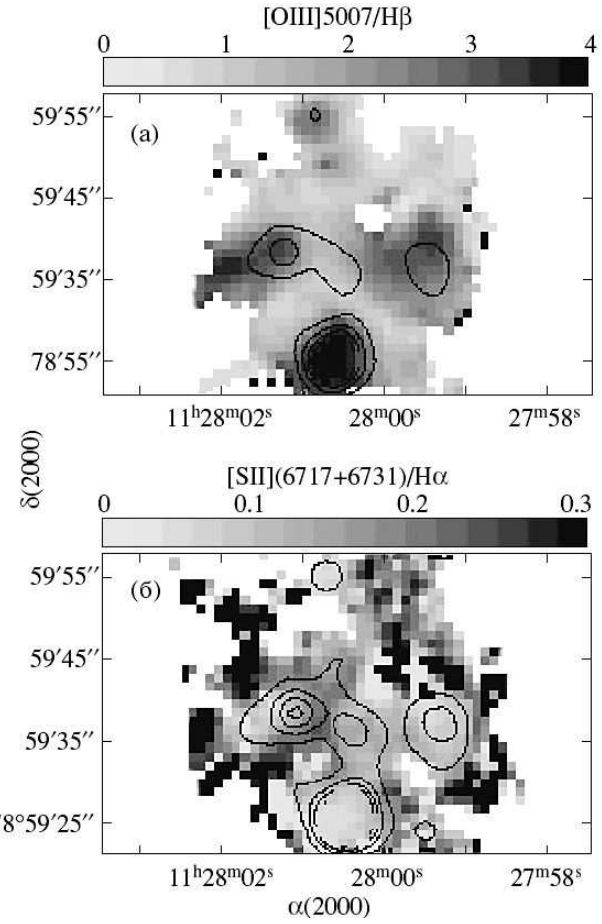

Fig. 3. Distribution of the relative line intensities, for (a) [OIII]λ5007/Hβ and (b) [SII]λ(6717+6731)/Hα. The contours show the image brightness in the (a) Hβ and (b) Hα lines. Darker shades indicate higher intensity ratios.

Introduction. The figure shows the part of the galaxy covered by our MPFS observations and the positions of the spectrograph slit. Images of the galactic central region in the Hα, Hβ, [SII]λ6717, 6731 Å, and [OIII] 5007Å lines obtained from MPFS observations are shown in Fig. 2.

Figure 3 displays maps of the distribution of the relative [OIII]/Hβ and [OIII]/Hβ line intensities based on these observations, traditionally used for diagnostics of the emission from HII regions and gas behind shocks. The contours in Figs. 3a and 3b show the brightness of the images in the Hβ and Hα lines, respectively.

It follows from Fig. 3 that the preliminary conclusion made in [1] that the relative [OIII]/Hβ and [OIII]/Hβ line intensities were enhanced inside the giant ring, between bright HII regions Nos. 2 and 4, is not confirmed by our MPFS observations. (This conclusion in paper [1] was based on filter images of the galaxy in the corresponding lines.) The second, still fainter, region mentioned in [1] is outside the giant ring, and is not covered by our MPFS observations.

We determined the mean relative intensities of the 'diagnostic' lines in the five bright HII regions in two ways: from the observations with the MPFS integral-field spectrograph and from the longslit spectrograms. The line intensities in the bright part of the giant ring were measured only with the integral-field data. The results are given in Table 2, which also contains the data for the bright HII regions obtained by Lynds et al. [2] with a longslit spectrograph on the 4-m telescope of the Kitt Peak National Observatory. The longslit observations in both studies were obtained under similar conditions, and with the same slit position. The spectral resolution (estimated from sky lines) was $FWHM = 120\,\mathrm{km\,s^{-1}}$ in our study, comparable to that of [2]; the angular resolutions were the same, equal to 2″ (this was limited by seeing in our observations, and by the slit width in [2]).

Table 2 contains the formal uncertainties of the means. The actual accuracy of our measurements is clear from a comparison of the relative intensities in the slit spectra and MPFS observations. Here, the main cause of disagreement between the estimates obtained using these two methods is the different integration regions used when deriving the mean line intensities for each object. All the data in Table 2 remain uncorrected for extinction.

Table 2 presents the relative intensities for the [OIII] line for the central region and of the [SII] line for the periphery of HII region No. 1 (according to the diagram in Fig. 4). For all the other HII regions in Table 2, the line intensities derived from the MPFS observations were averaged for the whole nebula, so that the largest contribution is from the brightest region in the corresponding line.

Table 2 demonstrates that, when taken together, the three sets of observations (our MPFS and longslit observations and the data of [2]) cover a wide spectral range and are in good mutual agreement. The low [NII]/Hα line-intensity ratio we measured in the five HII regions is consistent with the galaxy-mean value of 0.027 given by Martin [6].

3.1. HII region No. 1: variation of relative line intensities with distance from the center

A trend of the relative [SII]/Hα line intensity increasing and [OIII]/Hβ decreasing from the centers of the HII regions to their edges can be noted in Fig. 3. We considered this effect for the results of our MPFS observations of the brightest region No. 1.

Figure 4a displays the dependence of the [SII]λ(6717+6731)/Hα line-intensity ratio and the distance R from the center of HII region No. 1. We averaged the relative intensities in annular zones at the same distances from the center, the vertical line in the figure corresponds to the boundary of shell No. 1 from the HST Hα image. A similar dependence on the distance from the center of the HII region is shown in Fig. 4b for the [OIII]λ5007/Hβ line-intensity ratio.

The increase in the [SII]/Hα and decrease in the [OIII]/Hβ line intensities with distance from the center detected in HII region No. 1 is simple to understand: this trend could indicate that the gas is in a higher ionization

Table 2. Relative line intensities in the spectra of the bright HII regions

Line	HII 1	HII 2	HII 3	HII 4	HII 5	Giant ring	Ref.
[OII]λ3729/[OII]λ3726	1.39 ± 0.11	1.43 ± 0.14	1.50 ± 0.08	1.37 ± 0.10	1.80 ± 0.23		[2]
[OII]$(3726+3729)$/Hβ	0.59 ± 0.02	2.26 ± 0.11	1.18 ± 0.03	1.71 ± 0.06	2.20 ± 0.12		[2]
[OIII]λ5007/Hβ	3.89 ± 0.01	1.65 ± 0.03	2.68 ± 0.01	2.59 ± 0.03	1.28 ± 0.03		[2]
[OIII]λ5007/Hβ	3.43 ± 0.05	1.72 ± 0.02	2.85 ± 0.03	2.78 ± 0.03	1.69 ± 0.01		*
[OIII]λ5007/Hβ	3.86 ± 0.02	1.79 ± 0.04	2.85 ± 0.02	2.82 ± 0.04	1.63 ± 0.07	1.32 ± 0.08	**
[OIII]λ4363/Hβ	0.064 ± 0.002		0.049 ± 0.006	0.063 ± 0.009			[2]
[OI]λ6300/Hβ	0.011 ± 0.003	0.04 ± 0.01	0.044 ± 0.005				*
[SII]$\lambda(6717+6731)$/Hα	0.066 ± 0.001	0.137 ± 0.001	0.123 ± 0.001	0.096 ± 0.001	0.137 ± 0.003		*
[SII]$\lambda(6717+6731)$/Hα	0.051 ± 0.001	0.140 ± 0.008	0.110 ± 0.003	0.092 ± 0.005	0.137 ± 0.008	0.162 ± 0.015	**
[SII]λ6717/Hα	0.028 ± 0.001	0.07 ± 0.012	0.06 ± 0.003	0.056 ± 0.005	0.076 ± 0.09	0.086 ± 0.015	**
[NII]$\lambda(6548+6583)$/Hα	0.024 ± 0.001	0.032 ± 0.001	0.024 ± 0.001	0.025 ± 0.003	0.038 ± 0.002		*
[NII]λ6583/Hα	0.013 ± 0.001	0.027 ± 0.001	0.022 ± 0.001	0.021 ± 0.001	0.034 ± 0.002		*
Hγ/Hβ	0.44 ± 0.01	0.50 ± 0.01	0.42 ± 0.01	0.47 ± 0.01	0.51 ± 0.02	0.00 ± 0.00	[2]
Hβ/Hα	0.313 ± 0.002	0.304 ± 0.005	0.307 ± 0.002	0.309 ± 0.004	0.255 ± 0.01	0.384 ± 0.013	**

* — our data from longslit spectra.
** — our MPFS data.

Table 3. Extinction and gas parameters in the giant HII regions of VII Zw 403.

Parameter	HII No. 1	HII No. 2	HII No. 3	HII No. 4	HII No. 5
c	0.165	0.035	0.26	0.09	0.2
N_e(SII), cm^{-3}	57	66	57	110	–
T_e(SII), K	10 000	10 000	10 000	10 000	10 000
T_e(OIII), K	14 500	–	14 900	16 200	–

state at the center of the HII region, near the compact OB association, than towards its edges. In particular, lines of sulfur in higher ionization states than SII dominate in the central region, while virtually all the sulfur at the outer edge of the HII region may be in the form SII. Similarly, the oxygen at the center is predominantly in the form OIII, and its degree of ionization is lower towards the periphery of the HII region.

Quantitative estimates of this effect are hindered by the insufficient angular resolution of our observations. The HST Hα images show that HII region No. 1 has a shell structure that is narrower than the angular resolution of our MPFS observations.

Generally speaking, the enhancement of the [SII] lines at the periphery of HII region No. 1 could also be partially due to a contribution from gas emission behind the shock front. Recall that we detected weak high-velocity rings in this particular HII region in [1]. However, this contribution is not large: the intensity of the wings detected at velocities up to $300-500\,\mathrm{km\,s^{-1}}$ is 2-5% of the maximum in the Hα and [OIII] lines.

3.2. Analysis of the HII-region parameters from the measured emission lines

We used the emission-line intensity ratios from Table 2 to estimate the parameters of the gas in the giant HII regions and to obtain very rough estimates of the corresponding abundances of oxygen, sulfur, and nitrogen. We estimated the electron densities using the mean intensity ratio of the [SII]λ6717, 6731Å doublet lines for each of the bright HII regions.

The electron temperature in the region of [OIII] emission was derived from the intensity ratio of the auroral and nebular [OIII] lines; the intensities of the λ4363Å auroral line, quoted in Table 2, were taken from [2]. Unfortunately, the λ4363Å line was not measured in HII regions Nos. 2 and 5. For the region of emission in the [SII] lines, we adopted the electron temperature $T_e = 10\,000$ K, which is generally characteristic of low-excitation zones.

The parameters of the gaseous components in the HII regions are collected in Table 3. To estimate the extinction, we used the intensity ratios of the Hβ and Hα lines from MPFS data, as well as measurements of the Hγ to Hβ line-intensity ratios from Lynds et al. [2]. The two extinction estimates coincide for HII region No. 1; for the other HII regions, Table 3 presents average values for the two studies.

The mean electron density of the gas in the studied HII regions measured from the [SII] lines is $60-70\mathrm{cm^{-3}}$, in full agreement with the estimates from the [OII] lines presented in [2].

We used the observations of HII region No. 1 to estimate the gas densities at the periphery of this region, $n_e = 120$ cm^{-3}, and at its center, $n_e = 30$ cm^{-3}. These results agree with the estimate [2] of the mean density for HII region No. 1, $n_e = 50$ cm^{-3}, based on measurements of [OII] lines.

Our estimate, based on the [OIII] lines, of the electron temperature near the center of HII region No. 1, in the

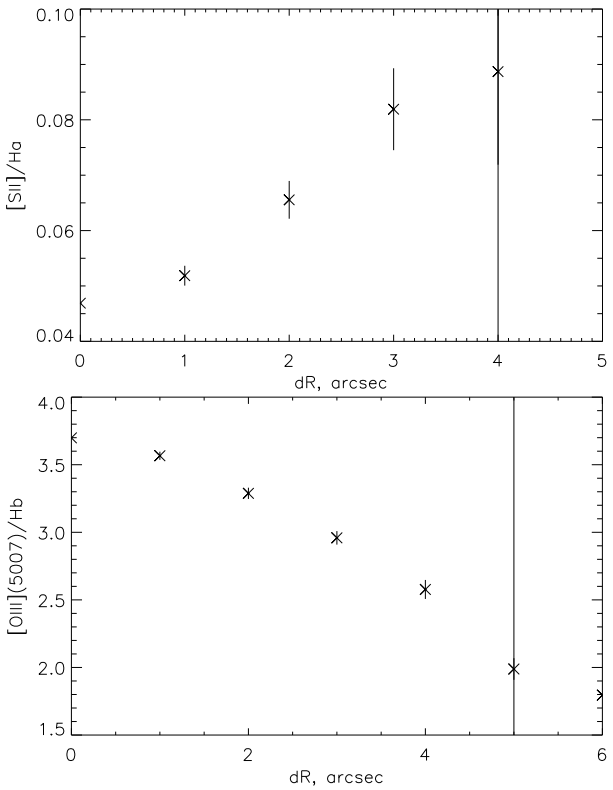

Fig. 4. Distribution of the relative line intensities, for (a) [SII]λ(6717+6731)/Hα and (b) [OIII]λ5007/Hβ line-intensity ratios versus distance R from the center of region No. 1. The vertical line is the boundary of shell No. 1 from the HST Hα image.

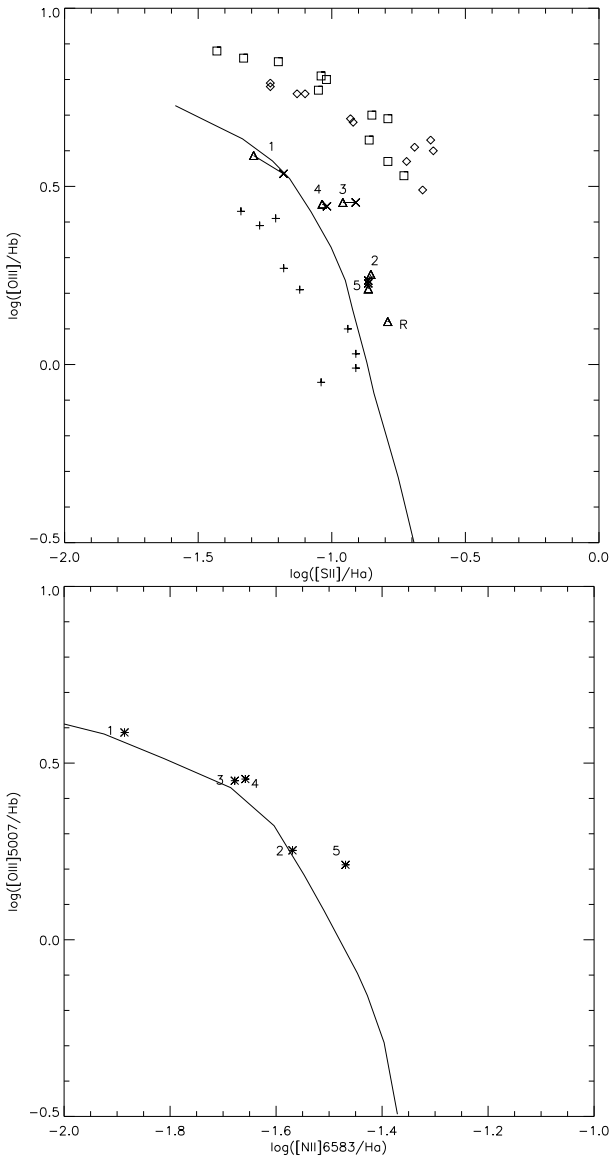

Fig. 5. Line intensity ratios from the MPFS (triangles) and longslit (crosses) data in the (a) [OIII]λ5007/Hβ–[SII]λ(6717+6731)/Hα and (b) [OIII]λ5007/Hβ–[NII]λ6583/Hα planes. The five bright HII regions are marked with their numbers, and the brightest part of the giant ring with the letter R. The solid curves are diagnostic relations derived by Dopita et al. [16]. Diagram (a) also shows measurements for HII regions in the dwarf galaxies I Zw 18 (pluses), II Zw 40 (squares), and NGC 4861 (diamonds) from Martin [6].

region of the highest intensity of doubly-ionized oxygen, is 14 500 K, in full agreement with the data of Lynds et al. [2], who obtained 14 000 $\pm$ 200 K K using the same method.

Our measured line-intensity ratios for the galactic five brightest HII regions and the brightest part of the giant ring are plotted in Fig. 5 in the [OIII]λ5007/Hβ–[SII]λ(6717+6731)/Hα and [OIII]λ5007/Hβ–[NII]λ6583/Hα planes. Figure 5a also shows the results for HII regions and diffuse ionized gas in other dwarf galaxies from [6]. We can see that the relative intensities of these lines in VII Zw 403 are typical of HII regions in dwarf galaxies.

Figure 5 also presents the diagnostic relations derived by Dopita et al. [16]. We do not use these diagnostic relations to estimate the gas metallicity in the galaxy for two reasons. First, the computations of [16] assumed a mass for the central cluster $M \geq 3 \times 10^3\ M_\odot$, while the compact associations in VII Zw 403 have lower masses. Second, the models were computed for a single burst of star formation, with the burst results traced for several Myr, while previous star-formation bursts can also be of crucial importance for the abundances of heavy elements in BCD galaxies (see below).

We can see in Fig. 5 that our observations of the five brightest HII regions in VII Zw 403 are consistent with the expected 'ionization sequence'. In fact, HII regions Nos. 1 and 4 are related to the richest compact OB associations, Nos. 1 and 5. According to [2], OB association No. 1 contains 25 blue stars with absolute MF555W magnitudes brighter than -4^m (main-sequence O stars; 27 after correction for incompleteness) and two type 1b red giants; the luminosity of the surrounding shell No. 1 (L(Hα) = 5×10^{50} photons/s) can be provided by these stars. Association No. 5 contains 28 stars with MF555W

brighter than -4^m (blue main-sequence stars and blue supergiants); the luminosity of the corresponding shell No. 4 ($L(\mathrm{H}\alpha) = 2.8 \times 10^{50}$ photons/s) is about 60% of the ionizing radiation from these stars. HII region No. 2 is related to the 'central' association (see Fig. 11 in [2]), and HII regions Nos. 3 and 5 to OB associations Nos. 4 and 6, respectively. Associations Nos. 4 and 6 are much poorer than No. 1 and No. 5 and contain nine and four blue luminous stars, respectively.

The position of the brightest region of the giant ring in the lowest part of the ionization sequence appears to correspond to the emission of diffuse ionized gas (as is observed in other galaxies analyzed by Martin [6]).

We attempted to use the measured line intensities to estimate the relative abundances of oxygen, sulfur, and nitrogen in the giant HII regions, understanding that the available data can yield only a very rough approximation.

Assuming that, as was demonstrated above for HII region No. 1, the oxygen near the center of each of the envelopes is in the state OIII, we can find the total oxygen abundance, assuming that OIII/HII $\approx$ O/H. We also assumed that the highest [SII]$\lambda(6717 + 6731)$/Hα and [NII]$\lambda(6548 + 6583)$/Hα ratios represented the total sulfur and nitrogen abundances, i.e. SII/HII $\approx$ S/H and NII/HII $\approx$ N/H. We derived the ion abundances of doubly-ionized oxygen and singly-ionized sulfur and nitrogen using the 'Five-Level' program of De Robertis et al. [17].

The resulting abundances of O, S , N in the galactic bright HII regions derived in this rough approximation are listed in Table 4. We can see that, on average for all five HII regions, the logarithmic oxygen abundance is $12 + \log(\mathrm{O/H}) = 7.4{-}7.6$, indicating an oxygen deficiency by a factor of 16–30 compared to the Sun. Sulfur is also relatively underabundant, by a factor of 13–30. The mean relative abundance of nitrogen, $12 + \log(\mathrm{N/H}) = 6.0 - 6.2$, corresponds to a deficiency by a factor of 80–120. The N/O relative abundance was found to be 0.03–0.04, also unusually low.

4. Discussion

Obviously, our spectral range is too narrow to provide accurate determinations of the galactic metallicity, and the above assumptions are very rough. However, the oxygen abundances we derived for the HII regions in the galaxy VII Zw 403 (with both the temperature and density being determined from lines for this element) are in very good agreement with the data of other studies. Martin [6] found the average value $12 + \log(\mathrm{O/H}) = 7.58 \pm 0.01$ for the galaxy. Introducing corrections for unobserved ionization states, Izotov et al. [18] found the galaxy average to be $12 + \log(\mathrm{O/H}) = 7.69 \pm 0.001$ Schulte-Ladbeck et al. [19] found the metallicity of the galactic gas to be $Z = (0.05{-}0.06)\ Z_\odot$.

Our assumption that oxygen near the center of an HII region is predominantly in the state OIII is confirmed by a comparison with the data in Table 4 of Izotov et al. [18], where the sum OII+OIII is given for the observed region of VII Zw 403, resulting in the same oxygen abundance as in our study.

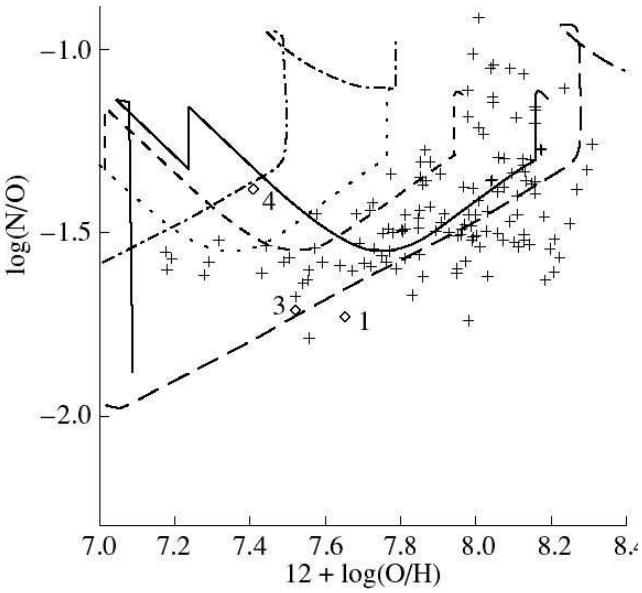

Fig. 6. Relative nitrogen and oxygen abundances derived for HII regions Nos. 1, 3, and 4 in VII Zw 403 and for other BCD and HII galaxies from [24, 25] in the $(12 + \log(\mathrm{O/H})) - \log(\mathrm{N/O})$ plane. The diagnostic diagrams suggested in [23] for four bursts of star formation are shown: the dotted curve corresponds to the star-formation rate $\nu = 0.2$ Gyr^{-1}, the short-dashed curve to $\nu = 0.3$ Gyr^{-1}, and the solid curve to $\nu = 0.3$ Gyr^{-1}. Also plotted are curves corresponding to two star-formation bursts from [20]: the dot-dashed curve corresponds to $\nu = 1$ Gyr^{-1}, and the long-dash curve to $\nu = 10$ Gyr^{-1}

The very low abundance of nitrogen relative to oxygen in the giant HII regions of VII Zw 403 can be explained in the models for the chemical evolution of BCD galaxies suggested by Brandamante et al. [20], Recchi et al. [21, 22], and Lafranchi and Matteucci [23] (see also references in [23]). According to these last authors, the observed heavy-element abundances in BCD galaxies can be understood in terms of the chemical evolution of these galaxies if there were several (two to seven) relatively short bursts of star formation separated by long 'quiescent' periods. Figure 6 displays the diagnostic diagrams in the $(12 + \log(\mathrm{O/H})) - \log(\mathrm{N/O})$ plane suggested in [23] for a model with four star-formation bursts at epochs corresponding to galaxy ages of 1, 11, 13, and 13.98 Gyr, with the burst durations being 20, 10, 200, and 20 Myr, respectively. The different curves correspond to different star-formation rates. Also shown are curves corresponding to two short bursts separated by a quiescent period for two extreme star-formation rates from Brandamante et al. [20].

Figure 6 shows the relative abundances we derived for HII regions Nos. 1, 3, and 4 using the parameters presented in Table 3 together with the results for other BCD and HII galaxies according to the data from Izotov and

Table 4. The relative abundances of oxygen, sulfur, and nitrogen in the giant HII regions of the galaxy VII Zw 403 compared to the Sun, in the $12 + \log(\mathrm{X/H})$ scale.

Element	HII No. 1	HII No. 2	HII No. 3	HII No. 4	HII No. 5	Sun
O	7.65		7.52	7.41		8.93
S	5.55	5.93	5.86	5.80	5.93	7.18
N	5.91	6.08	5.80	6.04	6.22	8.05
log(N/O)	–1.73		–1.71	–1.38		
log(S/O)	–1.82		–1.66	–1.62		

Thuan [24] and from Kobulnicky and Skillman [25].We see that the positions of HII regions Nos. 1, 3, and 4 in the diagnostic diagram agree with regions occupied by other galaxies of the same type and are consistent with the theoretical model of Lafranchi and Matteucci [23] with four star-formation bursts. Those authors note that the lowest N/O ratio is achieved during the third burst, explained by an increase in the oxygen abundance due to the injection of oxygen into the interstellar gas during massive type II supernovae explosions. (The injection of nitrogen 'lags behind' that of oxygen, since it is brought about by winds from lower-mass stars.)

It follows from Fig. 6 that, in the model with four star-formation bursts, our observations are consistent with the theoretical curves corresponding to the star-forming efficiency $\nu \approx 0.2{-}0.3$ Gyr^{-1}. This in no way contradicts any observations of VII Zw 403. Using the formula of Kennicutt [26] for estimating the current star-formation rate from a galactic Hα luminosity, we find from the value $L(\mathrm{H}\alpha) = (1.49{-}1.86) \times 10^{39}$ erg s^{-1} we derived in [1] the star-formation rate $(0.012{-}0.015)\ M_\odot$/yr for masses between 0.15 and 100 $M_\odot$. (Our measurements did not confirm the results of Silich et al. [7], who gave a much higher Hα luminosity for the galaxy (by a factor of 20), though our results are in good agreement with earlier measurements [2, 27].)

Given this star-formation rate and a total mass of gas in the galaxy near $10^8\,M_\odot$ (the HI mass estimated by Thuan and Martin [28] corrected for the new distance, 4.5 Mpc [2]), a gas-depletion time of about 8 Gyr corresponds to $\nu = 0.125\mathrm{Gyr}{-}1$. This is probably an upper limit; according to Bicker and Fritze-van Alvensleben [29], the use of the relation from [26], derived for the solar chemical composition, overestimates the star-formation rates of low metallicity galaxies.

The previous burst of star formation, which was responsible for the observed relative N/O abundance in the model of Lafranchi and Matteucci [23], was appreciably stronger than the current one. According to the model of [23], which is in good agreement with our observations, the last star-formation burst in VII Zw 403 commenced some 20 Myr ago. A detailed comparison of the galactic chemical evolution with the abundances of heavy elements observed in VII Zw 403 is beyond the scope of this study. We note only that multicolor stellar photometry with the HST suggests that several star-formation episodes with various intensities have occurred in the galaxy [2, 3].

Three epochs of active star formation in VII Zw 403 were identified in [3]. The first, identified from stars on the red-giant branch, occurred 3–10 Gyr ago, or possibly even earlier; the second burst, identified from stars on the asymptotic giant branch (AGB), occurred about 4 Gyr ago. The age of the third burst, which was responsible for the young stars and HII regions we observe today, does not exceed one Gyr.

Lynds et al. [2] also noted the rich population of AGB stars with ages of 1-5 Gyr, which is unusual for dwarf galaxies; the strongest starformation burst in VII Zw 403 happened between 800 and 600 Myr ago, possibly even 1.2 Gyr ago. The stars of this population dominate in the galaxy. The ages of six compact OB associations in the galactic central parts are about 4-6 Myr. (This estimate is fairly rough due to the small number of stars in the color-magnitude diagrams.) In addition to these compact associations, blue luminous stars are present in the galactic entire central field, out to a distance of one kpc. In particular, two stellar populations with ages of 5 and 10 Myr, or possibly somewhat more, are observed in the less compact stellar groups of mixed age, designated 'center', 'north', and 'south' in Fig. 11 of [2]. Thus, the stellar population of the galaxy exhibits signs of recent star formation that occurred in two bursts, about 5 Myr ago and about 10 Myr ago or somewhat earlier, with the strongest burst occurring 600-800 Myr ago (possibly about 1.2 Gyr ago), in complete agreement with the model of Lanfranchi and Matteucci [23] that provides the best approximation to our observational results for VII Zw 403.

Our study is the first to estimate the relative oxygen, sulfur, and nitrogen abundances for individual HII regions in VII Zw 403; results published earlier give the average chemical composition for the galaxy. The differences of the relative abundances $12 + \log(\mathrm{O/H})$ in HII regions Nos. 1, 3, and 4 of VII Zw 403 we have found (from 7.65 to 7.41; Table 4) are similar to the results obtained by Papaderos et al. [30] for the galaxy SBS 0335-052E. Both galaxies have similar Hα morphologies; in SBS 0335-052E, an O/H gradient between 7.20 and 7.31 on a scale less than one kpc was discovered. As for VII Zw 403, the highest oxygen abundance is observed in the brightest HII region of the galaxy, around the youngest cluster.

Acknowledgements. This study was supported by the Russian Foundation for Basic Research (project codes 04-02-16042 and 05-02-16454). The study is based on observations obtained at the 6-m telescope of the Special Astrophysical Observatory

(Russian Academy of Science), which is supported by the Ministry of Education and Science of the Russian Federation (registration number 01-43). The authors are grateful to O.K. Silchenko for helpful discussions.

References

[1] T.A. Lozinskaya, A.V. Moiseev, V.Yu. Avdeev, O.V. Egorov, 2006, Astronomy Letters, **32**, 361; (astro-ph/0605189)
[2] R. Lynds, E. Tolstoy, E.J. O'Neil, D.A. Hunter, 1998, ApJ, **16**, 146
[3] R.E. Schulte-Ladbeck, U. Hopp, M.M. Crone, L. Greggio, 1999, ApJ, **525**, 709
[4] T.X. Thuan, J.E. Hibbard, F. Levrier, 2004, AJ, **128**, 717
[5] T.X. Thuan, T.B. Williams, E. Malumuth, 1987, in: *Starburst and Galaxy Evolution*, Proc. of the 22-th Moriond Astrophys. Meeting, Les Arcs, France (Gif-sur-Yvette, Editions Frontieres), p. 151
[6] C.L. Martin, 1997, ApJ, **491**, 561
[7] S. Silich, G. Tenorio-Tagle, C. Muñoz-Tuñón, L.M. Cairõs, 2002, AJ, **123**, 2438
[8] P. Papaderos, K.J. Fricke, T.X. Thuan, H.-H. Loose, 1994, A&A, **291**, L13
[9] P. Lira, A. Lawrence, R.A. Johnson, 2000, MNRAS, **319**, 17
[10] D. Bomans, 2001, Rev. Mod. Astron., **14**, 297
[11] J. Ott, F. Walter, E. Brinks, 2006, MNRAS, **358**, 1423
[12] J. Ott, F. Walter, E. Brinks, 2006, MNRAS, **358**, 1453
[13] V.L. Afanasiev, S.N. Dodonov, A.V. Moiseev, 2001, in: *Stellar dynamics: from classic to modern*, eds L.P. Osipkov, I.I. Nikiforov (Saint-Petersburg Univ. Press), p. 103
[14] T.A. Kartashova, N.M. Chumakova, Astrofiz. Issled, 1978, **10**, 44
[15] V.L. Afanasiev, A.V. Moiseev, V. L. 2005, Astronomy Letters, **31**, 193; (astro-ph/0502095)
[16] M.A. Dopita, J. Fischera, R. Sutherland, L.J. Kewley, C. Leitherer, R.J. Tuffs, C.C. Popescu, W. van Breugel, B.A. Groves, 2006, ApJS, **167**, 177
[17] M. De Robertis, R. Dufour, R. Hunt, 1987, J. Roy. Astron. Soc. Canada, **81**, 195
[18] Yu.I. Izotov, T.X. Thuan, V.A. Lipovetsky, 1997, ApJS, **108**, 1
[19] R.E. Schulte-Ladbeck, U. Hopp, L. Greggio, M.M. Crone, 1999, AJ, **118**, 2705
[20] F. Bradamante, F. Matteucci, A. D'Ercole, 1998, A&A, **337**, 338
[21] S. Recchi, F. Matteucci, A. D'Ercole, 2001, MNRAS, **322**, 800
[22] S. Recchi, F. Matteucci, A. D'Ercole, M. Tosi, 2002, A&A, **384**, 799
[23] G.A. Lanfranchi, F. Matteucci, 2003, MNRAS, **345**, 711
[24] Yu.I. Izotov, T.X. Thuan, 1999, ApJ, **511**, 639
[25] H. Kobulnicky, E. Skillman, 1996, ApJ, **471**, 211
[26] R.C. Kennicutt, 1998, ARA&A, **36**, 189
[27] C.L. Martin, 1998, ApJ, **506**, 222
[28] T.X. Thuan, C.L. Martin, 1981, ApJ, **247**, 823
[29] J. Bicker, U. Fritze-van Alvensleben, 2005, A&A, 443, L19
[30] P. Papaderos, Yu.I. Izotov, N.G. Guseva, T.X. Thuan, K.J Fricke, 2006, A&A, **454**, 119

Translated by N. Samus'